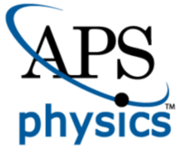

CHORUS

This is the accepted manuscript made available via CHORUS. The article has been published as:

Diffusion of Ag along Σ3 grain boundaries in 3C-SiC

Sarah Khalil, Narasimhan Swaminathan, David Shrader, Andrew J. Heim, Dane D. Morgan, and Izabela Szlufarska

Phys. Rev. B **84**, 214104 — Published 7 December 2011

DOI: 10.1103/PhysRevB.84.214104

Diffusion of Ag along Σ3 grain boundary in 3C-SiC

Sarah Khalil,* Narasimhan Swaminathan,* David Shrader,
Andrew J. Heim, Dane D. Morgan,† and Izabela Szlufarska†
Material Science Program, University of Wisconsin –Madison and
Material Science and Engineering Department, University of Wisconsin –Madison
(Dated: October 11, 2011)

Ag defects in Σ3 grain boundary of SiC were analyzed to test the hypothesis that Ag release from TRISO fuel particles can occur through grain boundary diffusion. Although Σ3 grain boundaries cannot provide a connected path through the crystal, they are studied here to provide guidance for overall trends in grain boundary vs. bulk Ag transport. Formation energies of Ag defects are found to be $2-4$ eV lower in the grain boundaries than in the bulk, indicating a strong tendency for Ag to segregate to the grain boundaries. Diffusion of Ag along Σ3 was found to be dramatically faster than through the bulk. At 1600°C, which is a temperature relevant for TRISO accident conditions, Ag diffusion coefficients are predicted to be 3.7×10^{-18} m^2/s and 3.9×10^{-29} m^2/s in the Σ3 grain boundary and bulk, respectively. While at this temperature Σ3 diffusion is still two orders of magnitude slower than diffusion estimated from integral release measurements, they values are close enough to suggest that grain boundary diffusion is a plausible mechanism for release of Ag from intact SiC coatings. The remaining discrepancies in the diffusion coefficients could be possibly bridged by considering high-energy grain boundaries, which are expected to have diffusivity faster than Σ3 and which provide a connected percolating path through polycrystalline SiC.

PACS numbers: 66.30.-h 61.72.Mm, 28.41.Bm

I. BACKGROUND

The cubic polytype of silicon carbide (3C–SiC) is one of the constituent materials in the design of TRistructural ISOtropic (TRISO) coatings for fuel particles in the very high temperature reactors (VHTR). In the current TRISO design, the 35 μm thick layer of 3C–SiC provides the main barrier to the escape of metallic fission products (MFPs) from the fuel core into the reactor coolant. Although the SiC layer retains most of the MFPs under operating and accident conditions, it releases some of the relatively long half-life MFPs, such as Ag (half-life 253 days) and Cs (30 years), which raises concerns about the reactor's safety. Numerous hypotheses have been proposed for the mechanisms underlying fast transport and release of MFPs through the SiC layer of TRISO, however no consensus has been yet reached on this issue. These hypotheses include chemical degradation of SiC[1,2], vapor diffusion through cracks and nano–pores[3–5], and diffusion along grain boundaries (GBs) and (pipe) dislocations[6,7]. Recently a number of studies have provided strong support for the hypothesis that GB diffusion is the dominant pathway for Ag transport[6,7]. For example Friedland *et al.*[4,8] carried out Ag implantation studies in a single crystal SiC and a polycrystalline SiC. It was observed that at 1300°C diffusion of Ag (measured by broadening of the Ag concentration profile) takes place in polycrystalline SiC, but not in a single crystal SiC. The results have been attributed to GB diffusion. More recently Lopez-Honorato *et al.*[9] designed a diffusion couple where Ag was trapped between two stoichiometric SiC layers and the samples were heat treated at temperatures of up to 1500°C. Significant diffusion was observed in the samples and transmission electron microscopy (TEM) images were consistent with the possibility that diffusion took place along GBs.

Previous atomistic studies on MFPs diffusion through SiC have focused on Ag diffusion through bulk SiC.[10]. It was found that in the absence of radiation damage Ag diffusion coefficient is low (6.9×10^{-35}m^2/s at 1200°C and 3.9×10^{-29}m^2/s at 1600°C for the fastest Ag defect) and therefore bulk diffusion cannot account for the experimentally observed release rates of Ag from TRISO particles.

Here we use atomistic modeling to determine quantitative differences between Ag diffusion along GBs and through the bulk of SiC. We also identify mechanisms that control diffusion of Ag along GBs. Our analysis is focused on the most common special GBs in 3C-SiC[11], which are the $\Sigma3\langle011\rangle\{211\}$ GBs. The overall goal of this study is to determine whether GBs in SiC can provide pathways for Ag diffusion with rates comparable to those reported in integral release measurements. Since the energy of $\Sigma3$ is low as compared to other GBs in SiC and there is some evidence that GBs with higher energies provide faster diffusion pathways [12,13], one can expect that $\Sigma3\langle011\rangle\{211\}$ twin GBs provide a lower bound estimate on GB diffusion in SiC.

In this paper it is important to keep in mind the distinction between Ag diffusion along a specific GB in SiC and diffusion through a polycrystalline sample of this material. The focus of this work is on the former issue. Diffusion through polycrystalline SiC, which is also critical for assessing long-range Ag diffusion and possible release from fuel particles, depends on how different GB paths are connected in a polycrystalline sample. In order to place our investigation in the context of experimental studies, we will compare diffusion values calculated for specific GBs to those measured for a polycrystalline material. Although a mesoscale microstructural model of diffusion is not the focus of the present work, a simplified analysis of how the diffusion coefficients for specific GBs can be mapped onto a polycrystalline material is given in Sec. IV. An example of a more complete mesoscale model of Ag transport in SiC can be found in Ref.[14].

II. SIMULATION METHODS

In our study we combine molecular dynamics (MD) simulations based on empirical potentials and *ab initio* calculations based on the Density Functional Theory (DFT). MD simulations are first employed to determine energetically most stable atomic configurations of $\Sigma3$ GBs. Relaxed GB structures are then used as an input for *ab initio* calculations of defect formation and migration energies. Finally these energies are used in combination with the Arrhenius relationship to calculate diffusion coefficients as a function of temperature.

A. Molecular dynamics

MD simulations are performed using the LAMMPS software package[15] and the Tersoff potential[16] with parameterization for SiC as proposed by Kohler *et al.*[17] This potential has been previously used by Wojdyr *et al.*[18] to model tilt GBs in 3C-SiC. GBs are investigated in a bicrystal configuration. The $\Sigma3$ GB lies in the $(2\bar{1}\bar{1})$ crystallographic plane and has a tilt axis aligned with the $[0\bar{1}1]$ direction. The initial GB structure is constructed so that no two atoms from different grains are at a distance less than 80% of the lattice parameter. The bicrystal structure is then optimized at high temperature using a procedure described in detail in Refs.[18,19]. The XZ cross-sectional structure

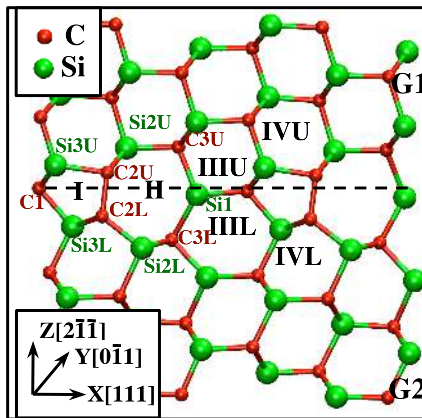

FIG. 1. A bicrystal GB model of $\Sigma 3 \langle 110 \rangle \{211\}$ GB. The dashed line corresponds to the GB plane separating the grains G1 and G2. Substitutional and interstitial sites are labeled by Arabic and Roman numerals, respectively. Sites in G1 and G2 are labeled as U and L, respectively. During relaxation, the Si1 column forms dimers along the Y direction. Coordination number is 4 for all atoms in the GB, which is the same as in the bulk SiC.

of the most stable $\Sigma 3$ GB structure is shown in Fig. 1, where X=[111] and Z=[2$\bar{1}\bar{1}$]. The Y direction is parallel to the GB tilt axis [0$\bar{1}$1]. The XZ cross-section in Fig. 1 is consistent with tight binding calculations and high resolution TEM images reported in the literature[20–24]. The stable structure of $\Sigma 3$ GB consists of 5-, 6-, and 7-membered rings, which are labeled I, III, and II, respectively. Atoms that form these GB rings occupy an approximately 5 Å thick slab centered at the GB. Atoms outside this slab are considered as belonging to crystalline grains (the bulk) of SiC. This definition of a GB is consistent with that considered in other studies on SiC[20].

B. Ab initio calculations

DFT-based *ab initio* calculations have been performed using the Vienna Ab-initio Simulation Package (VASP)[25–28]. We used the projector–augmented wave (PAW) method[29,30] and an energy cutoff of 450 eV for both Si and C atoms. All energies are calculated using a $1 \times 1 \times 1$ k-point mesh generated using the Monkhorst-Pack method[31] with consideration of the geometrical shape of the reciprocal space. The exchange–correlation functional was treated in the Generalized Gradient Approximation (GGA), as parameterized by Perdew, Burke, and Ernzerhof (PBE)[32]. The convergence criteria were set to 10^{-4} eV for the electronic self–consistency cycle. The forces in the ionic iterations were converged within ± 0.01 eV/Å. Migration barriers are calculated using the nudged elastic band (NEB) method. Formation energies E_{f} are calculated using the following formula:

$$E_{\mathrm{f}} = E_{\mathrm{def}} - E_{\mathrm{undef}} + \sum_{I} \Delta n_I \mu_I, \tag{1}$$

where E_{def} is the energy of a defected cell, E_{undef} is the energy of an undefected cell, Δn is the change in the number of atoms of species I from the perfect cell to the defected cell, and μ_I is the chemical potential of species I. For Si-rich conditions, μ_{Si} is equal to the energy of a Si atom in a Si crystal and μ_{C} is equal to the energy of a C atom in a SiC crystal. For C-rich conditions μ_{Si} is equal to the energy of Si atom in a SiC crystal and μ_{C} is equal to the energy of C in graphite. The values of all chemical potentials are taken to be the same as in Ref.[10]. In this paper we focus our discussion on Si-rich conditions. For charged defects, Eq. 1 contains additional terms related to electronic degrees of freedom (see for instance Ref.[10]). Since GB calculations are computationally expensive, in this study we only consider neutral defects. A discussion of how charged defects may impact our conclusions is presented in Sec.V.

Ab initio calculations are limited to relatively small system sizes. To perform such calculations, first a small system is cut out of a large structure that had been prepared and relaxed in MD simulations. The dimensions of the *ab initio* structure are chosen so as to maintain periodic boundary conditions within the plane of the GB. The lattice sites that overlap between the two grains in a bicrystal form a periodic structure within the GB plane, which structure is referred to as a coincidence site lattice (CSL). The size of the CSL unit cell is 7.55 Å and 3.08 Å along the X and Y directions, respectively. When discussing convergence of calculations, we label the system size by the number of CSL unit cells. For instance SiC 1×1 $\Sigma 3$ GB structure has one CSL unit cell in both, the X and the Y direction. The dimension along the Z direction is 18 Å for all samples considered in this study. This dimension is chosen to ensure that a reasonable number of bulk–like atomic layers are incorporated around the GB. Periodic boundary conditions

are applied in the X, Y, and Z directions of the bicrystal, where the Z direction has a free surface with a ~ 3 Å thick vacuum layer to avoid interactions between free surfaces. The two outermost layers of atoms parallel to the GB plane (perpendicular to the Z direction) are held rigid during *ab initio* calculations to prevent surfaces from an undesired reconstruction.

We tested the convergence of the calculations with respect to the system size using a $1 \times 1 \times 1$ k-point mesh. We calculated the formation energy of Ag on a Si site (Ag_{Si}) in $\Sigma3$ bicrystals with the following size: 1×2 (128 atoms), 2×1 (128 atoms), 2×2 (256 atoms) and 3×3 (384 atoms). We found that the formation energy E_f of this defect was converged to within 100 meV/defect for the 2×2 (256 atoms) system size with the $1 \times 1 \times 1$ k-point mesh. The 2×2 (256 atoms) system size will therefore be used throughout the entire study. Convergence with respect to the k-point mesh was also performed. For example, carbon vacancy (V_C) converged to within 150 meV/defect for a $1 \times 1 \times 1$ k-point mesh against a $3 \times 3 \times 3$ k-point mesh. The $1 \times 1 \times 1$ k-point mesh was then used for all further calculations.

C. *Diffusion coefficient calculations:*

The effective diffusion coefficient D^i_{eff} for a Ag defect of type i (e.g., a substitutional defect on the Si sublattice) migrating along GBs is assumed to follow the Arrhenius relationship

$$D^i_{\mathrm{eff}} = D^i_{\mathrm{eff},0}\ \exp\left(\frac{-Q^i_{\mathrm{eff}}}{k_b T}\right), \tag{2}$$

where k_b is the Boltzmann constant, T is the absolute temperature, $D_{\mathrm{eff},0}$ is a pre-exponential factor, and Q^i_{eff} is the effective energy barrier to diffusion. Q^i_{eff} and $D^i_{\mathrm{eff},0}$ are calculated by fitting the above equation (Eq. 2) to a plot of calculated D^i_{eff} vs. T^{-1}. The effective diffusion coefficient D^i_{eff} is calculated following the procedure from Ref.[33] as the product of an intrinsic diffusion coefficient D^i_{int} and a relative concentration of the defect i

$$D^i_{\mathrm{eff}} = D^i_{\mathrm{int}} \frac{C^i}{\sum_i C^i}. \tag{3}$$

Concentration (in defects per unit cell) of a defect of type i in the GB can be calculated as[34]

$$C^i = N^i \times \exp\left(\frac{-E^i_{\mathrm{f}}}{k_b T}\right), \tag{4}$$

where N^i is the number of sites of type i per unit cell of a GB and E^i_{f} is the formation energy of defect i. The intrinsic diffusion coefficient D^i_{int} quantifies the diffusivity of Ag in SiC, assuming Ag spends 100% of time as a defect of type i. D_{int} is approximated as

$$D^i_{\mathrm{int}} = D^i_{\mathrm{int},0} \exp\left(\frac{-Q^i_{\mathrm{int}}}{k_b T}\right), \tag{5}$$

where the pre-exponential factor $D^i_{\mathrm{int},0}$ is taken to be equal to $9.61 \times 10^{-8}\mathrm{m}^2/\mathrm{s}$. $D^i_{\mathrm{int},0}$ was calculated as the hop distance squared multiplied by an attempt frequency, assuming the attempt frequency to be equal to the phonon frequency of 10^{12} Hz and the hop distance to be equal 3.1 Å. Q^i_{int} is calculated from migration barriers, which in turn are determined using *ab initio* calculations (see Section III B for details).

To determine the diffusion coefficient D for transport of Ag through a polycrystalline SiC with an average grain diameter d, one needs to take into account both diffusion through crystalline grains (bulk), D_{bulk}, and diffusion along GBs, D_{GB}. The resulting diffusion coefficient can be estimated as[35]

$$D = \alpha_t D_{\mathrm{GB}} + (1 - \alpha_t)\, D_{\mathrm{bulk}}, \tag{6}$$

where α_t is the fraction of time that Ag atom spends in the GBs. This fraction of time can be in turn calculated as:

$$\alpha_t = \frac{g C_{\mathrm{GB}}}{g C_{\mathrm{GB}} + (1-g) C_{\mathrm{bulk}}}, \tag{7}$$

where g is the volume fraction of GBs, C_{GB} and C_{bulk} are concentrations of Ag atoms (in units of $1/\mathrm{m}^3$) in a GB and bulk SiC, respectively. The concentration C_{GB} of Ag defects in the GB is calculated as the sum $\sum_i C^i$ (where C^i is defined in Eq. 4) divided by the volume of a GB unit cell. C_{bulk} is calculated analogously based on energies from

TABLE I. Formation energies of vacancies, Ag substitutional and Ag interstitial in all possible sites in the GB and in bulk SiC[10].

Site	V_C (eV)	Ag_C (eV)	Site	V_{Si} (eV)	Ag_{Si} (eV)	Site	Ag_I (eV)
Bulk	4.13	7.39	Bulk	7.63	6.6	Bulk	10.49
C1	2.78	5.60	Si1	4.13	4.01	I	Unstable
C2U	1.97	3.63	Si2U	5.38	4.47	II	6.71
C2L	1.32	4.22	Si2L	5.02	4.74	IIa	4.70
C3U	2.49	4.59	Si3U	5.81	6.15	IIIL	5.99
C3L	2.31	4.76	Si3L	4.52	5.18	IIILa	3.27
C4U	2.66	4.99	Si4U	4.60	3.95	IVL	7.65
C4L	2.77	4.84	Si4L	4.32	3.69	IVLa	7.38

Ref.[10] Grain boundary volume fraction can be calculated as $g = V_{\mathrm{GB}}/(V_{\mathrm{GB}} + V_{\mathrm{bulk}})$, where V_{GB} and V_{bulk} are the volumes of GBs and bulk, respectively. V_{GB} is calculated as the GB thickness (5 Å) multiplied by the total area A_{GB} of the GBs in the sample. With a simple assumption that polycrystalline SiC consists of cubic grains with edge length d, we find $A_{\mathrm{GB}}/V_{\mathrm{bulk}} = 3/d$. In our calculations of the diffusion coefficient D (Eq. 6), we will assume $d = 0.8$ μm, which is a typical grain diameter in SiC microstructures used in the TRISO application. These assumptions yield $g = 0.0019$. D_{bulk} for Ag in 3C-SiC has been already calculated by Shrader *et al.*[10] Grain boundary diffusion coefficient D_{GB} can be calculated as

$$D_{\mathrm{GB}} = \sum_i D^i_{\mathrm{eff}} = \frac{\sum_i C^i D^i_{\mathrm{int}}}{\sum_i C^i}, \tag{8}$$

where index i represents different types of Ag defects.

This paper is structured as follows: first we calculate the energetics of Ag defects, including formation energies (E_{f}) and migration barriers (E_{m}), and we discuss the stability of Ag defects as dictated by their formation energies. Subsequently, for each defect i we calculate the intrinsic diffusion coefficient D^i_{int}, as well as the effective diffusion coefficient D^i_{eff} with the corresponding effective activation barrier Q^i_{eff} (Eq. 2). Q^i_{eff} is used to calculate the GB diffusivity (Eq. 8) and then the total diffusivity for Ag (Eq. 6). Values of Q^i_{eff} are then compared to those extracted from integral release measurements[4,36,37]. In this paper frequent reference to bulk defect formation energies will be made. All of the bulk values are taken from Shrader *et al.*[10].

III. RESULTS

The GB diffusivity is closely related to the atomic structure of the GB.[38] Within the thickness of the asymmetric GB, there are 14 physically distinct sites on the Si sublattice and 14 on the C sublattice. There are 14 symmetry distinct sites (7 on each sublattice), which are labeled as shown in Fig. 1. The additional 14 sites occupy a $(0\bar{1}1)$ plane that lies behind the $(0\bar{1}1)$ plane shown in Fig. 1. The structure of the asymmetric GB is comprised of columns of atoms extending along the Y $[0\bar{1}1]$ direction.

A. Defect formation energies

We determined formation energies of Ag point defects (i.e., interstitial Ag_I defects and substitutional defects Ag_{Si} and Ag_C formed on Si and C sublattices, respectively) as well as defect clusters $Ag_i + nV_j$ formed by Ag on the i sublattice and n vacancies on sublattice j. Because of the asymmetry, sites in G1 and G2 (see Fig. 1) are physically distinct. Since substitutional diffusion is vacancy mediated, calculating formation energies of Si and C vacancies is essential for determining the rate of Ag substitutional diffusion. All vacancy formation energies for the distinct sites labeled in Fig. 1 have been calculated and reported in Table I. Formation energies of Ag substitutional defects calculated for the same sites are also listed in Table I. Interstitials can occupy the free volume inside the GBs, which we refer to as pores. As shown in Fig. 1, within the GB thickness there are 4 distinct pores in the XZ plane, which are labeled I, II, IIIL, IIIU. In our calculations of interstitial formation and migration energies we additionally include Pore IV, which lies outside the GB region. Inclusion of Pore IV is necessary so that Ag can avoid Pore I during migration along the X[111] direction (Pore I is too small to stabilize Ag interstitial). Each of these pores has two distinct interstitial sites along the Y$[0\bar{1}1]$ direction, which leads to the total of 10 distinct interstitial sites that need to

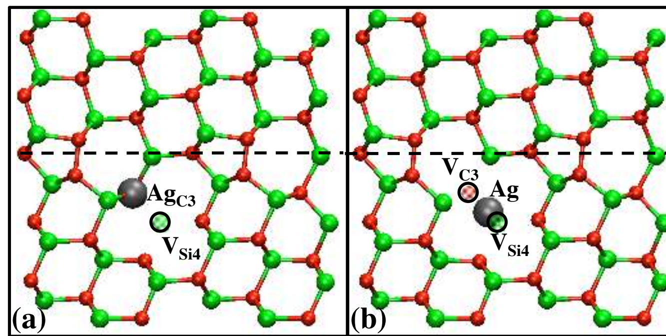

FIG. 2. (Color online) Ag + V cluster (a) before and, (b) after *ab initio* relaxation. For clarity, only one layer of atoms into the plane of the paper is shown.

be investigated. An additional label (a) is used to indicate distinct interstitial sites along the Y[0$\bar{1}$1] direction. In this notation, AgIIIL and AgIIILa denote two distinct Ag interstitials formed in pore IIIL. In Table I formation energies of Ag interstitials in the asymmetric GB are compared to the corresponding values in bulk. As might be expected, Pores IVL and IVLa, which are outside the pre-defined GB region and have the most bulk-like structure among the GB pores, have also the highest formation energies of interstitials (> 7 eV), closest to bulk values.

The most stable Ag interstitial is formed in Pore IIILa with the formation energy of $E_{\rm f} = 3.27$ eV. We found that there can be significant differences in formation energies between two interstitial sites along the Y[0$\bar{1}$1] direction. This difference is particularly large (~ 2.5 eV) for Pores IIIL and IIILa. The reason for this difference is a formation of Si dimers along the Y direction in the column Si1 (see Fig. 1). We found that formation energy of Ag interstitial next to the dimer is always higher than between two dimers. Another type of Ag defects considered in our study is a defect cluster. Clusters $\mathrm{Ag}_i + n\mathrm{V}_j$ are formed by a Ag atom on the i sublattice bound to n nearest-neighbor vacancies on the j sublattice. In our calculations we considered all combinations of Ag on substitutional sites given in Table I with all possible vacancy sites next to it. For clusters containing one vacancy, we found that both $\mathrm{Ag_{Si}} + \mathrm{V_C}$ and $\mathrm{Ag_C} + \mathrm{V_{Si}}$ relaxed to the same minimum energy configuration, which we will refer to as Ag + V. In the relaxed state the Ag atom resides along the line connecting the Si and C sites, and it is displaced from the Si site by 30% of the Si–C distance. An example of such a cluster before and after relaxation is shown in Fig. 2. Formation energies of Ag + V defects are in the range of $2.76 - 4.6$ eV (see Fig. 3).

Two-vacancy clusters $\mathrm{Ag}_i + 2\mathrm{V}_j$ were found to be more stable when i = Si and j = C. Specifically formation energies of $\mathrm{Ag_{Si}} + 2\mathrm{V_C}$ are in the range $3.74 - 5.73$ eV while formation energies of $\mathrm{Ag_C} + 2\mathrm{V_{Si}}$ are in the range $5.56 - 8.30$ eV. This trend can be explained by the fact that vacancies have significantly lower formation energies on C sublattice than on Si sublattice while Ag substitutionals have comparable formation energies on both sublattices (see Table I).

As we will show in Section III B the fastest diffusing Ag defect has effective energy barriers to diffusion $Q_{\rm eff}$ equal to 7.62 eV and 3.95 eV along the X and Y directions, respectively. Because formation energies of $\mathrm{Ag_C} + 2\mathrm{V_{Si}}$ defects are at least as high as ~ 5.56 eV, for this defect to become competitive with the fastest diffusing species along the X and Y directions, it would need to have values of $Q_{\rm int}$ lower than ~ 2 eV and lower than zero, respectively. Since such a scenario is not likely (or even possible for the negative migration energy), our analysis of migration energies will be focused only on the $\mathrm{Ag_{Si}} + 2\mathrm{V_C}$ clusters.

Overall we found that the single vacancy clusters are more stable than the di-vacancy clusters. In addition clusters are more stable in the GB than in the bulk. The most stable Ag + V in the GB has the formation energy lower by 2.56 eV than the most stable neutral cluster in bulk ($\mathrm{Ag_{Si}} + \mathrm{V_C}$) and lower by 0.7 eV than $\mathrm{Ag_{Si}} + \mathrm{V_C}$ in its most energetically favorable charge state (-1) in bulk. The $\mathrm{Ag_{Si}} + 2\mathrm{V_C}$ and $\mathrm{Ag_C} + 2\mathrm{V_{Si}}$ clusters are also more stable in the GB (see Fig. 3) than in the bulk, where the corresponding bulk energies are 6.44 eV and 11.4 eV.

We define a binding energy E_b of a cluster as the difference between the formation energy of a defect cluster and the sum of formation energies of its point defect constituents. If the binding energy is negative, the constituents of the cluster favor being bound together and a positive binding energy means that a cluster is unstable with respect to its constituents. Similarly as in the bulk SiC[10], we find that there is a strong binding tendency between Ag and the participating vacancies in a $\mathrm{Ag}_i + n\mathrm{V}_j$ cluster. In addition binding energies are comparable for clusters of the same type. For example, the Ag + V clusters have binding energies of -5.89 ± 0.63 eV, the $\mathrm{Ag_{Si}} + 2\mathrm{V_C}$ clusters have binding energies -4.80 ± 0.87 eV and the $\mathrm{Ag_C} + 2\mathrm{V_{Si}}$ clusters have binding energies of -7.71 ± 0.91 eV. Although binding energies of the $\mathrm{Ag_C} + 2\mathrm{V_{Si}}$ cluster are the largest, this is the least stable cluster because of the high formation energies of Si vacancies. It is notable that formation energies of the Ag + V cluster are lower than of Ag substitutional defects. We attribute the low formation energy of this cluster to the large binding energy between Ag and V. This

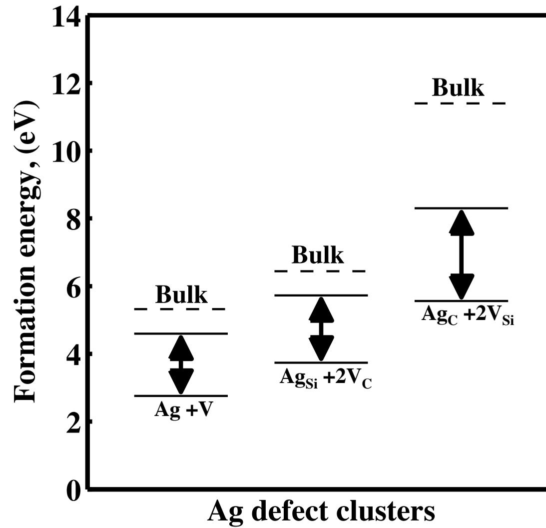

FIG. 3. The range of formation energies of Ag defect clusters in the Σ3 GB. Bulk values correspond to neutral defects reported in Ref.[10]

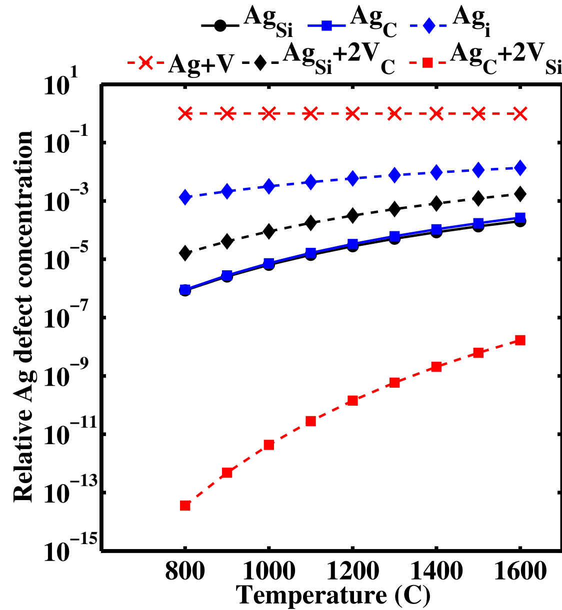

FIG. 4. (Color online) Relative concentrations of different defect types in the Σ3 GB as a function of temperature.

propensity of Ag to attract a V is presumably due to the size of a Ag atom (covalent radius of 1.45 Å[39]), which is significantly larger than Si and C atoms (covalent radii of 1.11 Å and 0.76 Å, respectively[39]). The presence of a nearby vacancy relaxes the strain introduced by Ag into the SiC lattice. As shown in Fig. 3, adding another vacancy to form $Ag_{Si} + 2V_C$ increases the defect formation energy, which suggests that the additional free volume created by the second vacancy is not energetically beneficial enough to the Ag to overcome the energy required to create the vacancy.

In Figure 4 we plot the relative concentrations of all types of Ag defect in the Σ3 GB as a function of temperature for the range of temperatures relevant to VHTR and TRISO applications. To calculate these relative concentrations, we take into account all possible defect sites within the unit cell of a GB. The concentration of Ag defects can be calculated from their formation energies using Eq. 4. By far the most stable Ag defect is found to be the $Ag + V$ cluster.

In order to better understand the implications of the the GB defect energetics, it is useful to compare the formation

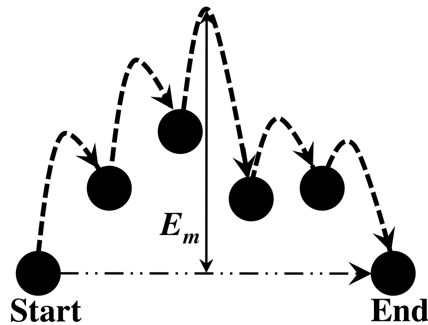

FIG. 5. A schematic diagram of a path for Ag diffusion between two symmetry equivalent positions. E_m corresponds to the migration energy for this diffusion path.

energies of Ag defects in the Σ3 GB to the formation energies of Ag in bulk SiC. Generally, we found that vacancies on the C sublattice are more stable than on the Si sublattice in both the Σ3 GB and bulk SiC. In the GB, the most stable vacancy is found on C_{2L} with the formation energy lower by 2.87 eV than that of a neutral C vacancy in the bulk. Formation of substitutional Ag defects on both C and Si sublattices in the GB are found to be more stable in the GB than in bulk by $\sim 1-4$ eV. The formation energy of the most stable Ag substitutional defect in the GB (Ag_c) is lower by 3.76 eV than the energy of the most stable Ag substitutional in the bulk. Interstitial formation energies are also lower in the GB. Specifically, the most stable Ag interstitial occupies Pore IIILa and its formation energy is lower by 7.22 eV than the most stable neutral interstitial in the bulk (see Table I). The significant reduction in the formation energies of GB defects compared to bulk indicates a strong segregation tendency of Ag atoms to the Σ3 GB. In addition, since the high formation energies of Ag interstitial and Si and C vacancies were some of the key energies that made diffusion in bulk slow[10], reduction in these energies suggests that substitutional and interstitial diffusion of Ag might be significantly enhanced in the GB as compared to bulk.

Having calculated formation energies of all Ag defects in the GB, we are now in a position to determine the fraction of time α_t that Ag spends in the Σ3 GB (Eq. 7) at the operating temperature of VHTR (1200°C). First we calculate $C_{\mathrm{GB}} = 9.4 \times 10^{18}$ m^{-3} and $C_{\mathrm{bulk}} = 3.03 \times 10^{10}$ m^{-3}, which gives a segregation factor $s = C_{GB}/C_{bulk} \approx 3.1 \times 10^{8}$. The value of C_{GB} has been calculated based on energies of neutral defects from Ref.[10] Assuming an average grain diameter of $d = 0.8\mu$m we determine $\alpha_t = 0.999998$, which shows that there is a very strong tendency for Ag to segregate to GBs in SiC. Consequently when calculating the diffusion coefficient D through a polycrystalline SiC sample, it is reasonable to assume $\alpha_t = 1$ and the second term in Eq. 6 to be equal zero, that is $D \approx D_{\mathrm{GB}}$.

B. Diffusion

Following the sequence of investigations in this paper, we first explore possible diffusion mechanisms of Ag point defects (interstitial and substitutional) and then extend the discussion to Ag defect clusters. For each diffusion mechanism we begin by identifying possible diffusion paths along the complex structure of a GB. Each diffusion path is characterized by a number of hops that connect two symmetry equivalent sites as shown in Fig.5. If a given defect type i has multiple paths j, the intrinsic diffusion barrier Q_{int}^{ij} is first determined separately for each path. All considered paths are investigated starting from the site where the defect is most stable. We define a complete diffusion path as the path between two symmetry equivalent sites in the GB. The intrinsic migration barrier E_{m}^{ij} of Ag along the entire path j is estimated as the energy difference between the lowest formation energy E_{f}^{ij} (starting point of the path) and the maximum energy state of the defect along this path (see Fig. 5).

Because diffusion along GBs is typically anisotropic[40], separate investigations have been carried out for diffusion along the X[111] direction (perpendicular to the tilt axis of the GB) and the Y[0$\bar{1}$1] direction (parallel to the tilt axis) (see Fig. 1). We first consider diffusion along the X[111] direction, dividing the discussion into substitutional, interstitial and cluster diffusion.

For substitutional diffusion the intrinsic energy barrier can be estimated as[41]

$$Q_{\mathrm{int}} = E_f^{\mathrm{V}} + E_b^{\mathrm{Ag+V}} + \left(E_m^{\mathrm{Ag/V}}\right), \tag{9}$$

where $E_{\mathrm{f}}^{\mathrm{V}}$ is the vacancy formation energy, $E_{\mathrm{b}}^{\mathrm{Ag+V}}$ is the binding energy of Ag and a vacancy on the first nearest neighbor sites of the same sublattice, $E_{\mathrm{m}}^{\mathrm{Ag/V}}$ is either the migration barrier of Ag or the vacancy, depending on which

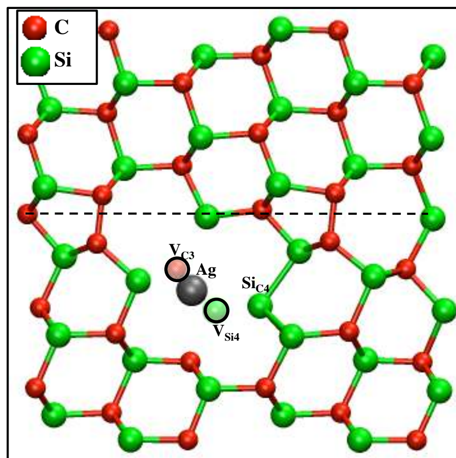

FIG. 6. *Ab initio* relaxation of a Ag_C and a V_C after relaxation, where the Si atom moves to V_C forming Si_C leaving behind a V_{Si}. For clarity, only one layer of atoms into the plane of the paper is shown.

one is larger. Generally, vacancy hopping barriers on the carbon sublattice are in the range of $\sim 3.5-6$ eV. Paths with the lowest vacancy migration barriers are investigated first. When investigating substitutional diffusion along the X[111] direction, we found that a vacancy on the C sublattice is unstable next to Ag on the C sublattice. This vacancy relaxes to the nearest neighbor Si site while Si atom moves to the C site and forms an antisite (see Fig. 6). In contrast, we found that Ag_{Si} next to a V_{Si} is stable. The corresponding defect configurations had values as low as $Q_{int} = 4.63$ eV which is ~ 2.5 eV lower than Q_{int} of other defects we investigated (see Table II). However, due to the higher formation energies of V_{Si}, Q_{eff} for Ag_{Si} diffusion was significantly higher than Q_{eff} for of the fastest defects. The larger stability of the $Ag_C + V_{Si}$ cluster suggests that Ag will diffuse as a cluster rather than as a substitutional atom. Cluster diffusion is discussed later in this section.

For Ag interstitial diffusion, hopping along the X[111] direction involves migration barriers in the range of $\sim 1-5$ eV. Formation energies along the diffusion path are as high as ~ 7.5 eV (Pore IV). Since Ag interstitial must pass through Pore IV to complete a path along the X [111] direction, this high formation energy will always be a limiting barrier to the diffusion along the X[111] direction. The fastest diffusion path we found has an intrinsic migration barrier of 7.12 eV.

It is instructive to compare interstitial diffusion in the GB to that in bulk SiC. Shrader *et al*[10] found that Ag interstitial diffusion through bulk SiC was slow because of the high formation energy (10.49 eV) of these defects. Because formation energy (E_f) of Ag interstitials is reduced in the $\Sigma3$ GB by ~ 7.22 eV, Q_{eff} will also be reduced as compared to the bulk and the interstitial diffusion could be enabled in the GB. However, the rate of diffusion of Ag interstitial depends also on the migration barriers (and therefore on the intrinsic energy barriers Q_{int}). The lowest intrinsic energy barrier along the X[111] direction was found to be $Q_{int} = 7.12$ eV, which is much higher than the 0.89 eV value in the bulk. Consequently Q_{eff} for Ag interstitial in the GB is 7.62 eV, which is comparable to the bulk value of 7.88 eV. Interstitial diffusion is slowed down in the GB along the X[111] direction by the high migration barriers rather than formation energy as in the case of bulk SiC.

The $Ag + V$ cluster has a number of possible configurations along the X[111] direction because of the presence of distinct (Si/C) sites. A migration path along the X direction will include these different cluster arrangements, which have formation energies in the range from 2.76 eV to 4.76 eV. In our analysis we considered all possible paths for $Ag + V$ diffusion along the X[111] direction. Starting from the defect with the lowest formation energy, we calculated all of the hops that make a complete diffusion path to a symmetry equivalent site. All diffusion paths were found to involve one or more of the following rate limiting defect states: (i) formation of a Si/C antisite, (ii) hopping of two atoms simultaneously, and (iii) unbinding of the vacancy from the cluster. For instance the binding energy of the vacancy to the most stable $Ag + V$ cluster is -6.29 eV and therefore unbinding of a vacancy from a cluster requires overcoming a high energy barrier. We found that the path with the lowest intrinsic barrier for diffusion along the X[111] direction has $Q_{int} = 7.56$ eV. Since this $Ag + V$ is also the most stable defect in the GB (see Fig. 4) is it not surprising that its $Q_{eff} \approx Q_{int} = 7.56$ eV.

We have also investigated diffusion of $Ag_{Si} + 2V_C$ cluster, where we started by calculating the rate limiting defect states for the possible paths along the X[111] direction. We found that the lowest rate limiting barrier has the value of ~ 10 eV, which makes $Ag_{Si} + 2V_C$ diffusion too slow to compete with other Ag defects. Comparing the diffusion coefficients for Ag defects along the X[111] direction in Table II, we conclude that $Ag + V$ cluster mechanism

TABLE II. Summary of the fastest diffusion mechanisms of each Ag defect type i migrating along the X[111] direction in the $\Sigma 3$ GB. Reported values correspond to 1200°C.

Ag defect i	Q^i_{int} (eV)	Q^i_{eff} (eV)	$D^i_{\mathrm{eff},0}$ (m^2/s)	D^i_{eff} (m^2/s) 1200°C
$\mathrm{Ag_C}$	Unstable			
$\mathrm{Ag_{Si}}$	> 4.63	> 10.49	$\sim 10^{-9}$	$< 10^{-44}$
$\mathrm{Ag_I}$	7.12	7.62	9.79×10^{-8}	8.31×10^{-34}
$\mathrm{Ag + V}$	7.56	7.56	3.18×10^{-7}	4.33×10^{-33}
$\mathrm{Ag_{Si} + 2V_C}$	> 10.00		$\sim 10^{-8}$	$< 10^{-42}$

TABLE III. Energies used to determine the fastest Ag substitutional diffusion path. Si(n-na) refers to hopping between sites Si(n) and Si(na) along the Y direction on column n. Q_{eff} is calculated using Eq. 2 after calculating D_{eff} using Eq. 3. Q^{ij}_{int} which is needed to calculate D_{int} and hence D_{eff} is obtained from Eq. 9.

	$E^{\mathrm{V}}_{\mathrm{f}}$ (eV)	$E^{\mathrm{Ag}}_{\mathrm{f}}$ (eV)	$E^{\mathrm{Ag+V}}_{\mathrm{b}}$ (eV)	$E^{\mathrm{Ag/V}}_{\mathrm{m}}$ (eV)	Q^{ij}_{int} (eV)
C(1-1a)	2.78	5.60	−1.81	3.78	4.75
C(2-2a)	1.32	4.22	−0.53	6.16	6.95
C(3-3a)	2.59	4.76	−3.32	2.70	1.97
Si(1-1a)	4.13	4.01	−0.32	2.90	6.71
Si(2-2a)	5.02	4.74	−0.45	3.70	8.27
Si(3-3a)	4.52	5.18	0.71	3.08	8.31
Si(4-4a)	4.36	3.69	−0.53	4.36	8.19

is the fastest Ag diffusion mechanism along the X[111] direction of the $\Sigma 3$ GB with a Q_{eff} =7.56 eV and D_{eff} of 4.33×10^{-33} m^2/s at 1200°C.

We found that Ag diffusion along the Y$[0\bar{1}1]$ direction is typically faster than along the X[111] direction. Since most of the formation energies in Table I suggest that energetics of grain G2 are lower than energetics of the grain G1 (See Fig. 1), we limited our diffusion rate calculations to G2. As shown in Table III, substitutional diffusion on C sites is generally faster than on Si sites, largely because of the high formation energy of $\mathrm{V_{Si}}$. Among C atoms, column C2 has the lowest formation energies for both $\mathrm{V_C}$ and $\mathrm{Ag_C}$. However diffusion on this column is relatively slow due to high migration energies (6.16 eV). The fastest substitutional diffusion takes place on the C3 column, which has the second lowest formation energy for $\mathrm{V_C}$, the largest binding energy (-3.32 eV) and the lowest migration barrier (2.70 eV). The corresponding energy barrier is $Q_{\mathrm{eff}} = 3.95$ eV (see Table IV) and the diffusion coefficient is $D_{\mathrm{eff}} = 4.88 \times 10^{-21}$ m^2/s at the reactor operating temperature of 1200°C and $D_{\mathrm{eff}} = 3.69 \times 10^{-18}$ m^2/s at 1600°C, which is the accident temperature of VHTR. Diffusion of the Ag interstitial along the Y$[0\bar{1}1]$ direction involves migration along one of the pores shown in Fig. 1. We calculated migration barriers for Ag interstitial along three pores II, III, and IV. Pore I is too small for Ag interstitial to be stable in it. Both the formation energies of Ag interstitial (see Table I) and the corresponding migration barrier (4.83 eV) are the lowest in Pore III. The estimated D_{eff} at 1200 °C $\leq T \leq$ 1600 °C ranges between 5.69×10^{-26} m^2/s and 4.44×10^{-22} m^2/s. Diffusion of the Ag interstitial along the Y$[0\bar{1}1]$ direction was found to be ~ 8 orders of magnitude faster than interstitial diffusion along the X [111] direction.

There are two possible paths for diffusion of Ag + V along the $[0\bar{1}1]$ direction, the zigzag and the ladder paths (see Fig. 7). Step-by-step mechanisms of cluster diffusion along these paths are shown in Fig. 8 and Fig. 9, respectively. The main difference between the two mechanisms is that the ladder path requires unbinding of the vacancy while the

TABLE IV. Summary of the fastest diffusion mechanisms of Ag defect i migrating along the Y$[0\bar{1}1]$ direction in the $\Sigma 3$ GB. The values of diffusion coefficients for $\mathrm{Ag_C}$ and $\mathrm{Ag_{Si}}$ correspond to columns C3 and Si1, respectively.

Ag defect i	Q^i_{int} (eV)	Q^i_{eff} (eV)	$D^i_{\mathrm{eff},0}$ (m^2/s)	D^i_{eff} (m^2/s) 1200°C
$\mathrm{Ag_C}$	1.97	3.95	1.60×10^{-7}	4.88×10^{-21}
$\mathrm{Ag_{Si}}$	6.71	7.94	1.60×10^{-7}	1.09×10^{-34}
$\mathrm{Ag_I}$	4.83	5.33	9.80×10^{-8}	5.69×10^{-26}
$\mathrm{Ag + V}$	5.58	7.65	9.79×10^{-8}	6.56×10^{-34}
$\mathrm{Ag + 2V}$	4.45	6.55	9.80×10^{-8}	3.81×10^{-30}

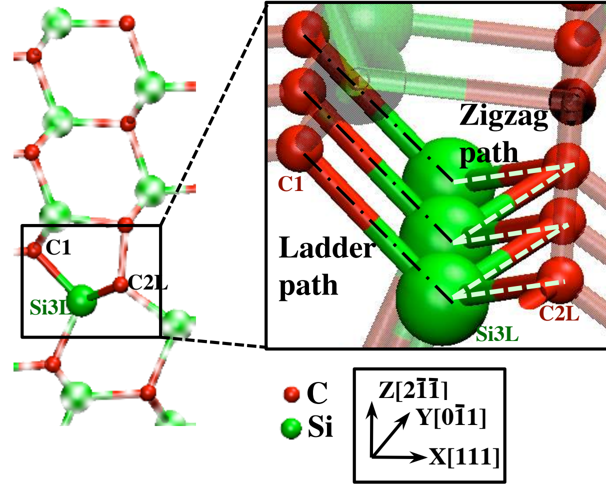

FIG. 7. (Color online) CSL unit cell in Σ3 GB: (a) 2D model (b) A 3D segment of the GB showing atoms the zigzag and ladder paths for cluster diffusion.

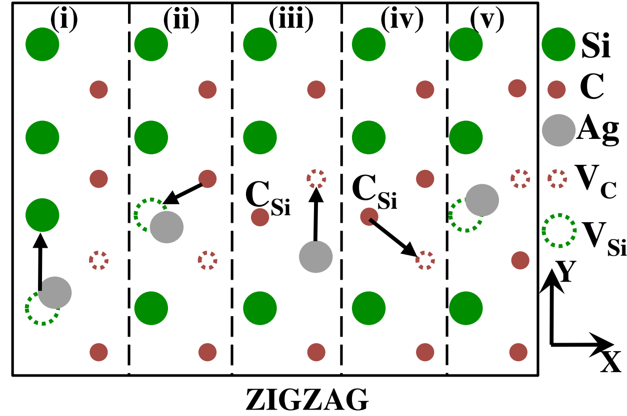

FIG. 8. (Color online) Schematic picture of the "zigzag" mechanism associated with moving the Ag + V cluster along the [0$\bar{1}$1] direction. Arrows indicate directions where atoms will move to form the next configuration to the right.

zigzag path does not. Since unbinding of the vacancy has a high energy barrier, it is not surprising that we found Q_{int} to be lower for the zigzag path, which will be described here in detail. We start by placing a Ag atom on the C sublattice (C2) and a vacancy on the Si sublattice (Si3). This configuration relaxes so that Ag occupies an intermediate position between two vacancies V_{Si3} and V_{C2} (configuration (i) in Fig. 8). Subsequent steps are schematically shown in Fig. 8 where configuration (v) is symmetry equivalent to (i). The rate limiting barrier for this path was found to be between configurations (ii) and (iii). We found that for the zigzag path $Q_{\mathrm{int}} = 5.58$ eV (see Table IV) and $D_{\mathrm{eff}} = 6.56 \times 10^{-34}$ m^2/s at 1200 °C. The ladder mechanism, which is schematically shown in Fig. 9, was found to have $Q_{\mathrm{int}} = 9.16$ eV. This value is ~ 3.5 eV higher than Q_{int} of the zigzag mechanism. It is also higher by ~ 1.6 eV than diffusion of the Ag + V cluster along the X[111], although for all other defect types considered diffusion along the X direction was slower. We also identified the possible paths for diffusion of $\mathrm{Ag_{Si}} + 2\mathrm{V_C}$ along the Y[0$\bar{1}$1] direction. The formation energies of $\mathrm{Ag_{Si}} + 2\mathrm{V_C}$ clusters were found to be in the range of $3.74 - 5.73$ eV (see Fig. 3), which values are larger but comparable to the formation energies of other defects. Specifically, the most stable $\mathrm{Ag_{Si}} + 2\mathrm{V_C}$ defect has a formation energy ~ 1 eV higher than the most stable Ag + V defect, 0.11 eV higher than $\mathrm{Ag_C}$, 0.05 eV higher than $\mathrm{Ag_{Si}}$, and 0.47 eV higher than Ag_I. We found that the migration paths for the $\mathrm{Ag_{Si}} + 2\mathrm{V_C}$ defects involve rate limiting steps that are similar to those found for the Ag + V cluster and that include unbinding of a vacancy from the cluster, simultaneous swapping of two atoms, and formation of an antisite. Here we discuss the migration path and migration energies of the most stable $\mathrm{Ag_{Si}} + 2\mathrm{V_C}$ defect, which is $\mathrm{Ag_{Si2}} + \mathrm{V_{C2}} + \mathrm{V_{C3}}$. The path is schematically shown in Fig. 10. The rate limiting barrier for this mechanism is the step between configurations (i) and (ii), which

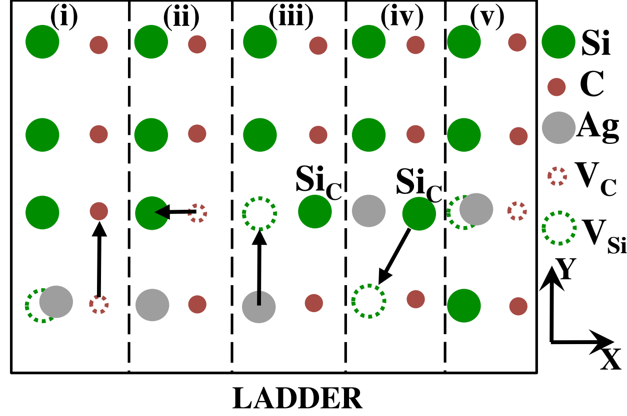

FIG. 9. (Color online) Schematic picture of the "ladder" mechanism associated with migration of the Ag + V cluster. Arrows indicate directions where atoms will move to form the next configuration to the right.

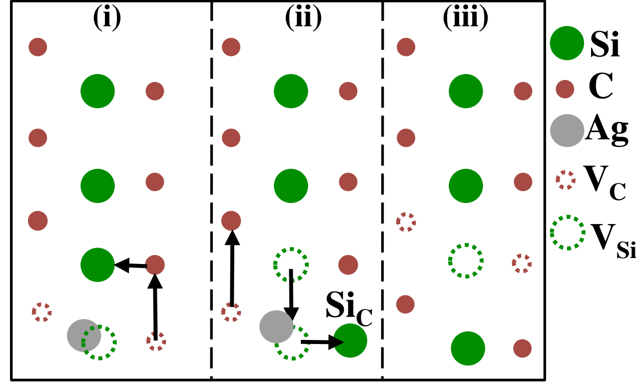

FIG. 10. (Color online) Schematic representation of the mechanism for diffusion of $Ag_{Si} + 2V_C$ along the Y $[0\bar{1}1]$ direction. Arrows indicate directions where atoms will move to form the next configuration to the right.

involves separation of V_{C3} from the cluster and a formation of the antisite Si_{C3}. Formation energies of configurations (i) and (ii) are 3.74 eV and 9.19 eV, respectively, and the activation barrier between these configurations is 4.45 eV. The estimated $Q_{\rm eff}$ (see Table IV) for this mechanism is approximately 6.55 eV, which is ~ 1 eV lower than $Q_{\rm eff}$ for the fastest diffusion path of the Ag + V cluster along the Y$[0\bar{1}1]$ direction. In general we found that although defect clusters (such as Ag + V) can be very stable in the $\Sigma3$ GB (see Fig. 4), these clusters have relatively high energy barriers $Q_{\rm int}$ for diffusion (Table IV). This trend is similar to what has been found in bulk SiC[10] and the migration paths of clusters involve similar rate limiting steps as in the bulk. We found that the fastest Ag defects in the GB are substitutional defects. For substitutional diffusion on the C sublattice $Q_{\rm eff}$ =3.95 eV, which value is signifantly lower than the corresponding energy in bulk SiC ($Q_{\rm eff}$ = 7.88 eV). The reason why this barrier is high in bulk is the high formation energy of vacancies[10] This is yet another indication that vacancy concentration plays an important role in the diffusion of Ag along the $\Sigma3$ GB.

IV. COMPARISON OF AG SOLUBILITY AND DIFFUSIVITY WITH EXPERIMENTAL INTEGRAL RELEASE

To understand how the *ab initio* predicted values of the formation energies and the diffusion coefficients in this work relate to existing data from integral release[36,37,42,43] and ion implantation[4] experiments, we first compare activation energies for diffusion and then construct a model that predicts integral release rates based on our calculations.

In Fig. 11, we compare activation energies $Q_{\rm eff}$ for diffusion coefficients calculated in this paper to those previously reported in the literature for Ag transport in SiC. The data for bulk SiC corresponds to *ab initio* calculations from Shrader *et al*[10]. In addition we plot a dashed line that corresponds to the lower bound on the effective energy barrier

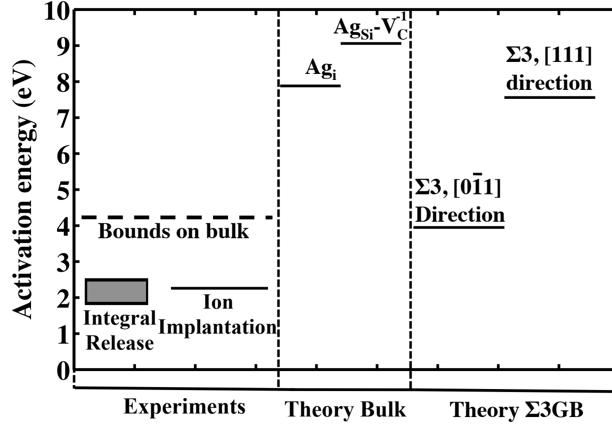

FIG. 11. Activation energies reported in literature of Ag diffusion through SiC. Integral release data is taken from Refs[36,37,42,43], ion implantation studies from Ref.[4], *ab initio* calculations of Ag diffusion through bulk from Ref.[10], and GB data is taken from this work.

for bulk diffusion, as determined from experiments where bulk diffusion was not observed during the time of the measurement[4,5]. These bounds are consistent with calculations for bulk diffusion by Shrader *et al*[10]. We also include data for experimentally measured integral release from TRISO-coated fuel particles [36,37,42,43]. These measurements have activation energy for diffusion approximately between 1.83 and 2.26 eV. A similar activation barrier (~ 2.5 eV) for diffusion of Ag in a polycrystalline SiC has been found in ion implantation studies by Friedland *et al*[4]. Figure 11 shows that bulk SiC has the highest Q_{eff} and that Q_{eff} for the $\Sigma 3$ is higher than the value obtained from integral release measurements by more than $\sim$ 1.69 eV. Calculations for $\Sigma 3$, which is a special GB with a bulk-like local atomic environment, provide an estimated lower bound on the GB diffusion in SiC. Less ordered (high-energy) GBs are expected to provide more stable locations and faster diffusion pathways.

While data shown in Fig. 11 is useful for comparing diffusion coefficients from different studies, for the Ag fission product to be released from the TRISO particle's SiC layer, the Ag atoms must first dissolve in SiC. The solubility of the Ag in SiC can be determined using the calculated formation energies of Ag defects. To estimate Ag release rates we construct a model that predicts integral release values as a function of formation energies and diffusion coefficients. We then constrain this expression to yield integral release values consistent with experiment, thereby defining the possible formation energies as a function of the diffusion coefficients. This method is somewhat approximate but provides a simple way to understand the observable implications of Ag solubility and transport in SiC.

In our model we assume that Ag diffusion occurs along columnar GBs that extend radially from the center of the particle through the SiC layer and therefore the integral release can be calculated as $\text{IR} = \Phi t (A_f^{gb} 4\pi {r_i}^2)$. In this expression Φ stands for the Ag flux, A_f^{gb} is the fractional area of the internal surface of SiC that consists of GBs (i.e., the fraction of the internal areas through which flux can pass), r_i is the inner radius of the SiC layer in the TRISO coating, and t is time. The flux Φ can be derived as follows. The SiC is a nearly spherical shell with an inner and outer surface. We then approximate the SiC as a flat layer, ignoring the relatively small effects associated with its curvature on the transport modeling. We assume that the diffusion of Ag through the SiC is along GB paths with boundary conditions for Ag concentration c being equal to the solubility limit and zero at the inner and outer surface of the SiC layer, respectively. With these assumptions the steady state flux of Ag through the SiC is $\Phi = D_{\text{eff}}^{\text{Ag}} \nabla c = D_{\text{eff}}^{\text{Ag}} c_{\text{Ag}} / d_{th}$, where $D_{\text{eff}}^{\text{Ag}}$ is the effective diffusion of Ag through SiC, d_{th} is the thickness of the SiC layer, and c_{Ag} is the solubility limit of Ag in SiC. Further, it is assumed that no time is spent diffusing through the TRISO components other than the SiC (e.g., the fuel and carbon layers). All of the relevant symbols and values needed for derivation of our model are summarized in Table V.

It is worth mentioning that previous integral release calculations have used a different model, developed by Booth[44]. We differ from that approach in that the Booth model has no Ag solubility term and solves for spherical diffusion through the entire particle (not just through radial GBs in SiC as in our model). Also, the Booth model solves for fractional release in terms of an evolving flux while our model assumes the flux is always maximal, given the solubility limit of Ag in SiC. In order to relate the results of our flux model to the integral release data, we need an estimate of how much Ag is produced and released in a typical integral release experiment. The typical amount of Ag produced is estimated as follows. Assuming a low enriched UO_2 kernel with a density of $10.93 \frac{\text{g}}{\text{cm}^3}$ and taking recent TRISO particle dimensions as given in Table V, we estimate that there are $\sim 1.82 \times 10^{17}$ U atoms in the kernel. If we consider

TABLE V. Definitions and values for parameters used to estimate Ag release from simple diffusion model.

Property (Symbol) [units]	Value	Comments
SiC properties		
GB width (d_{gb}) [Å]	5	This work
Grain diameter (d) [μm]	0.8	This work
Molar density (ρ) [mol/m^3]	1.6×10^5	Ref.[45]
Fractional area of GB (A_f^{gb})	$\approx 2d_{gb}\times\frac{d}{d^2} = \frac{2d_{gb}}{d}$	Cubic grains
TRISO particle properties		
Fuel Kernel radius (r_k) [m]	1.75×10^{-4}	Ref.[46]
SiC thickness(d_{th}) [m]	3.5×10^{-5}	Ref.[46]
Tortuosity (τ)	2	Ref.[47]
Inner radius of SiC (r_i) [m]	3.15×10^{-4}	Ref.[46]
Total Ag in fuel ($n_{\rm Ag}$) [mol]	5.03×10^{-11}	See discussion
Time to 10% release (t_{10}) [sec]	10 days $=8.64\times10^5$	Ref.[1,48]
Ag in Si properties		
Formation energy of Ag ($E_f^{\rm Ag}$) *ab initio*[eV]	4.76(Table I)	Ag in site C3L
Ag solubility limit ($c_{\rm Ag}$) [mol/m^3]	$\rho\exp(\frac{-E_f^{\rm Ag}}{kT})$	Analytic expression
($D_{\rm eff}^{\rm Ag}$) at 1600°C Ag diffusivity in SiC [m^2/s]	a) 8.07×10^{-19} b) 3.69×10^{-18} c) $(4-76)\times10^{-16}$	a) Ion implantation[4] b) $\rm Ag_{C3L}(\Sigma3)$ Table IV c) Integral release[36,37,42,43]
Ag flux through SiC (Φ) [mol/m^2-s]	$D_{\rm eff}^{\rm Ag}\times\frac{c_{\rm Ag}}{d_{th}\tau}$	

the kernel to have completed 10% fissions per initial metal atoms (FIMA) and assume a yield of 0.166% Ag per fission event[49], we estimate that the total number of moles of Ag in the kernel is $n_{\rm Ag}=5.03\times10^{-11}$. Now, by assuming that 10% of Ag release happens in time t_{10} and that Ag is entirely mediated by the diffusion through the SiC layer, we can write

$$0.1n_{\rm Ag}-\Phi t_{10}(A_f^{gb}4\pi {r_i}^2)=0. \tag{10}$$

Substituting $\Phi=D_{\rm eff}^{\rm Ag}c_{\rm Ag}/d_{th}$ and $c_{\rm Ag}=\rho\exp\left(-E_f^{\rm Ag}/kT\right)$, the above equation can be rewritten as

$$E_f^{\rm Ag}=-\ln\left(\frac{0.1n_{\rm Ag}d_{th}\tau}{\rho t_{10}D_{\rm eff}^{\rm Ag}A_f4\pi r_i^2}\right)k_bT. \tag{11}$$

Figure 12 shows (black line) the functional relationship from Eq. 11 for a temperature of 1600°C, which is the accident temperature in the VHTR and as well as a typical temperature for integral release experiments. Points on the line denote the fastest diffusion coefficients determined in this work for the $\Sigma3$ GB ($\rm Ag_C$ along Y direction), experimental values determined by ion implantation[4], as well as the range of values estimated from integral release experiments[36,37,42,43]. These diffusion coefficients are also calculated for 1600°C. For the GB data we give the numerical value of formation energy that solves Eq. 10 and we also show (in parentheses) the corresponding formation

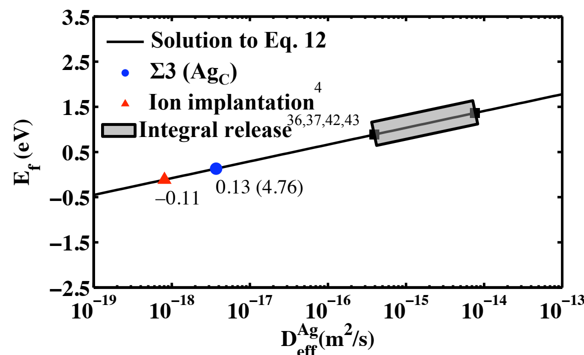

FIG. 12. The black line shows the implicit relation between the formation energies (ordinate) and diffusivity of Ag (abscissa) in SiC implied by Eq. 10. The circle on the line corresponds to our calculated values for the fastest Ag diffusion coefficients from either the X or Y direction in the Σ3 GB. The values in parenthesis are the corresponding formation energies (from a source of bulk Ag metal) calculated in this work for each GB type using *ab initio* methods. The triangle shows the point on the line corresponding to the diffusion coefficients from ion implantation[4] while the shaded grey region shows the extent of the line associated with the several diffusion coefficients obtained from integral release experiments [36,37,42,43]. The negative formation energies are not physical and simply represent that the diffusion coefficients considered are too low to yield a physical solution to Eq. 10

.

energy obtained from our *ab initio* calculations (from Table I). If the two values are comparable, that means that the *ab initio* and integral release data are consistent.

It should be pointed out that the formation energies depend on the Ag chemical potential of the Ag in the TRISO fuel just as it enters the SiC, which is difficult to determine rigorously. This chemical potential is likely associated with Ag in some form of gaseous state or sorbed into carbon, possibly bound to an anionic species like oxygen or iodine. A thorough study of the Ag reference state under realistic TRISO conditions is beyond the scope of this paper so here we estimate the plausible range of Ag chemical potential. One common approach to estimate a chemical potential in such situation is to find an upper bound for the chemical potential based on stability arguments. Here we consider two possible upper bounds.

The first possible upper bound we consider is bulk metallic Ag. To support this upper bound one argues that the Ag source in TRISO is more stable than bulk metallic Ag or bulk metallic Ag would form and pin the chemical potential at the bulk Ag value. By this argument bulk Ag provides an upper bound on the Ag chemical potential. Bulk Ag is already the reference state used to determine all of the *ab initio* formation energies in this paper. Therefore, with the bulk Ag upper bound, the calculated *ab initio* formation energies of Ag given in this paper can be treated as lower bounds on the true Ag formation energies expected in the fuel particle (i.e., the real formation energy would be more positive, leading to lower solubility). However, it should be noted that the preceding argument only holds if the Ag can equilibrate with itself during the release process. The small amount of Ag created and released, approximately 3×10^{13} atoms (see Table V), means that Ag may not interact enough to form bulk Ag. Under this scenario it is possible for Ag atoms to have chemical potentials much higher than bulk Ag. For this reason, a more conservative upper bound is considered.

The second possible upper bound we consider is an isolated Ag atom. To support this upper bound one argues that if the Ag were less stable than an isolated Ag atom, the Ag could always form a gas of Ag atoms, which at finite temperature would have a chemical potential significantly lower than the isolated Ag atom due to entropic terms. By this argument an isolated Ag atoms provides an upper bound on the Ag chemical potential. Our calculated Ag cohesive energy relative to the isolated (spin polarized) atom is 2.50 eV. Therefore, if this upper bound is used then all the formation energies calculated for Ag presented in this paper would decrease by 2.5 eV per Ag. This upper bound is very conservative as it assumes Ag cannot bind significantly to any available sites, which seems unlikely. We will therefore generally use the bulk metallic Ag to estimate our Ag chemical potential and invoke the more conservative At atom value to assess if results might be sensitive to the exact Ag chemical potential.

The trend of the line in Fig. 12 shows that higher formation energies (lower solubility) require higher diffusion coefficients to still yield overall transport consistent with experiments. It can be seen from Fig. 12 that the formation energy predicted by the diffusion coefficient of the Ag_C defect in the Σ3 GB (circle) is 0.13 eV and that predicted by ion implantation studies (triangle) is negative (-0.11 eV). The negative formation energies are not physical and demonstrate that the measured diffusion coefficients are too low to explain the Ag integral release even if Ag were 100% soluble in SiC.

While the formation energy derived from Eq. 10 for the Σ3 GB is positive, the value of 0.13 eV is still extremely low. It is 4.63 eV lower than what was obtained (4.76 eV) from direct *ab inito* calculation of Ag formation energies in the Σ3 GB in this work. This discrepancy would persist even if we use the Ag atom reference state, in which case the calculated formation energy change from 4.76 eV to 2.26 eV. However, it should be noted that the effect of neglecting charge in defect formation energies for the Ag+V cluster (which is the fastest defect in Σ3 GB) can be on the scale of ~ 2 eV (see Ref[10]), which could conceivably lower the formation energy for Ag in the Σ3 GB to values consistent with integral release data. That said, such an alignment of all the uncertainties in our predictions seems unlikely. Therefore, even though the Σ3 GB presents a region with far more solubility and diffusion than the bulk SiC[10], the diffusion coefficient and formation energy for the Σ3 GB do not allow for quite enough transport to fully explain the integral release data. Other hypothesis to explain this remaining discrepancy with the experimental Ag release are discussed in Sec. V.

It is interesting to note in Table IV that for the Σ3 GB the value of Q_{int} for Ag_C (1.97 eV) is similar to the migration barriers predicted from integral release experiments[36,37,42,43] (between 1.83 eV and 2.26 eV) or ion implantation measurements[4](2.5 eV). However, as pointed out above, the formation energies of Ag in the fastest diffusing path, which makes use of C3L sites, is 2.2 eV higher than the most stable state of Ag (the Ag-V cluster) in the Σ3 GB (Table I and section III.A). Therefore, despite the low value of Q_{int} , the D_{eff} of Ag_C is too low to provide adequate Ag mobility to explain the integral release data.

V. DISCUSSION AND CONCLUSION

We investigated to what extent GBs in SiC can provide faster diffusion pathways for Ag as compared to bulk SiC. In order to do that we calculated diffusion coefficients for migration of Ag along the Σ3 ⟨011⟩ {211} GB, which because of the special bulk-like structure of this GB provides an approximate lower bound on diffusion coefficient along GBs in SiC. The results were compared to bulk studies previously reported by Shrader *et al.*[10]. We found that for a typical grain diameter (0.8 μm) of SiC used in TRISO application there is a strong segregation of Ag to the Σ3 GB. Specifically, we found that, based on Σ3 energies, the fraction of time that Ag spends in the GB is 99.999% at 1200°C and 99.988% at 1600°C. This strong segregation, combined with the slow diffusion in bulk SiC[10], means that GB pathways will dominate diffusion of this fission product through a polycrystalline SiC (assuming no cracks or pores that enable faster diffusion are present). In the above calculations we used formation energies of neutral defects both in the GB and in the bulk.

Diffusion along the Σ3 GB was found to be anisotropic with a faster migration along the Y[0$\bar{1}$1] direction than along the X[111] direction. The fastest mechanism was found to be a substitutional diffusion on the C sublattice along the Y direction with the effective energy barrier $Q_{\text{eff}} = 3.95$ eV. The corresponding diffusion coefficients are $D_{\text{eff}} = 4.88 \times 10^{-21}$ m^2/s (at the operating temperature of 1200°C) and $D_{\text{eff}} = 3.69 \times 10^{-18}$ m^2/s (at the accident temperature of 1600°C). Within this range of temperatures, diffusion of Ag along Σ3 is $11 - 14$ orders of magnitude faster than diffusion through bulk[10]. We found that the diffusivity along the Σ3 GB in SiC is $2-3$ orders of magnitude slower than the fastest diffusion reported from fitting to integral release measurements (see Table V). Given that Σ3 provides an approximate lower bound on diffusion, it is plausible that other types of GBs will be able to account for the remaining discrepancy between diffusion coefficients. Even a small enhancement in the GB diffusivity would mean that GBs could explain the experimentally observed release of Ag in SiC. In particular calculations need to be carried out for random high-energy GBs, which are most likely to form a percolating path through SiC and which are characterized by a large amount of structural disorder. These random GBs constitute a majority ($> 50\%$) of GBs in CVD grown SiC[11]. This % fraction of GBs is more than sufficient to provide a percolating path through a material based on the following argument. It has been found that the percolation behavior of GB paths is similar to those for paths of nearest-neighbor bonds on the fcc lattice[50] and percolation of first nearest-neighbor bonds on the fcc lattice occurs with just 11.9% of bonds occupied[51]. It is reasonable to assume that high-energy GBs will provide pathways for Ag diffusion with rates faster than those found for special GBs (such as Σ3), as such behavior have been found for impurities diffusing in other materials[12,13]. Other phenomena that might reduce the gap between diffusion coefficients calculated for Σ3 GBs and those estimated from integral release measurements are enhancement of GB diffusion due to irradiation and an increased solubility of Ag in SiC GBs due to co-incorporation with other impurities present in the environment.

It is important to point out that some of the defects in bulk must be modeled as charged, that is it is necessary to add (remove) electrons to (from) the defect to obtain the lowest formation energy. We did not consider charged defects in the GB, and by calculating segregation factors, we assumed that the effect of charge on formation energies cancels between the bulk and the GB. It is in principle possible that the magnitude of the energy reduction due to the charging of defects would be lower in the GB than in the bulk and therefore the segregation effect would not be as strong as predicted in this paper. In the limiting case when charged and neutral defects have the same energy in

the $\Sigma3$ GB, the segregation factor would be 1.17×10^2 and Ag would spend only $\sim 18\%$ of time in the GB. Although this hypothetical scenario would have a significant effect on segregation tendency, the impact on the effective diffusion coefficient in a polycrystalline SiC would be small (see Eq. 6). This small effect is because diffusion through bulk ($D_{\text{eff}} = 6.9 \times 10^{-35}$ at 1200°C) is orders of magnitude slower than diffusion along the GBs.

Our calculations show that Ag diffusion along $\Sigma3$ GBs of SiC is significantly faster than diffusion in the bulk. It is instructive to ask what physics has changed when Ag segregated from bulk to the GB. By comparing our results to studies of Ag diffusion in bulk SiC[10], we idenfity the following differences between bulk and GB diffusion:

1. In bulk SiC Ag has a high formation energy (10.49 eV) of interstitials. Even though the intrinsic diffusion barrier for interestitials is low (< 1 eV), the high formation energy makes the effective energy barrier to diffusion high ($Q_{\text{eff}} = 7.88$ eV). In the $\Sigma3$ GB, interstitial formation energies are reduced by ~ 7 eV, which is why interstitial diffusion could possibly become active. This reduction is related to a larger free volume available for interstitials in the GB as compared to the bulk. The effective barrier for interstitial diffusion is reduced by ~ 2.5 eV, which means that interstitials are indeed faster in the GB, although not as fast as the substitutional defects.

2. In bulk SiC Ag has a high migration barriers for clusters ($Q_{\text{int}} = 9.10$ eV). Although $\text{Ag}_{\text{Si}} - \text{V}_{\text{C}}$ clusters are stable in bulk ($E_f = 5.32$ eV) relative to other Ag defects, unbinding of a vacancy from Ag and formation of an antisite defect are energetically expensive processes that limit migration of this cluster. The $\text{Ag} + \text{V}$ cluster is more stable in the GB (by ~ 2.56 eV as compared to a neutral cluster in the bulk) due to a reduction in the vacancy formation energies. However, migration of a cluster involves a similar rate limiting step as in the bulk and the overall diffusion rate of the $\text{Ag} + \text{V}$ is not significantly faster in the GB than it is in the bulk.

3. As shown in Eq. 9, vacancy formation energy contributes to the intrinsic energy barrier for substitutional diffusion. In bulk SiC vacancies formation energies are 7.63 eV for V_{Si} and 4.13 eV for V_{C}. These high values prevent substitutional diffusion in the bulk[10]. In $\Sigma3$, vacancy formation energies are reduced appreciably with values of 4.13 eV and 1.32 eV for V_{Si} and V_{C}, respectively. Substitutional diffusion of Ag on the C sublattice becomes particularly fast ($Q_{\text{eff}} = 3.95$ eV) and this mechanism dominates Ag transport along the $\Sigma3$ GB.

ACKNOWLEDGMENTS

The authors gratefully acknowledge support from the Department of Energy NERI Grant No.DE-FC07-07ID14823. They also acknowledge Dr. Yutai Katoh of ORNL for helpful comments on the study.

---

[*] These authors contributed equally to the paper.
[†] Corresponding authors: szlufarska@wisc.edu; ddmorgan@wisc.edu
[1] K. Minato, K. Sawa, T. Koya, T. Tomita, A. Ishikawa, C. A. Baldwin, W. A. Gabbard, and C. M. Malone, Nucl. Technol. **131**, 36 (2000).
[2] W. Schenk, G. Pott, and H. Nabielek, J. Nucl. Mater **175**, 19 (1990).
[3] K. Minato, T. Ogawa, K. Fukuda, H. Sekino, H. Miyanishi, S. Kado, and I. Takahashi, J. Nucl. Mater. **202**, 47 (1993).
[4] E. Friedland, J. B. Malherbe, N. G. van der Berg, T. Hlatshwayo, A. J. Botha, E. Wendler, and W. Wesch, J. Nucl. Mater. **389**, 326 (2009).
[5] H. MacLean, R. Ballinger, L. Kolaya, S. Simonson, N. Lewis, and M. Hanson, J. Nucl. Mater. **357**, 31 (2006).
[6] R. E. Bullock, J. Nucl. Mater **125**, 304 (1984).
[7] D. Petti, J. Buongiorno, J. Maki, R. Hobbins, and G. Miller, Nucl. Eng. Des. **222**, 281 (2003).
[8] E. Friedland, N. van der Berg, J. Malherbe, J. Hancke, J. Barry, E. Wendler, and W. Wesch, J. Nucl. Mater. **410**, 24 (2011).
[9] E. López-Honorato, D. Yang, J. Tan, P. Meadows, and P. Xiao, J. Am. Ceram. Soc. **93**, 3076 (2010).
[10] D. Shrader, S. Khalil, T. Gerczak, T. Allen, A. Heim, I. Szlufarska, and D. Morgan, J. Nucl. Mater. **408**, 257 (2010).
[11] L. Tan, T. Allen, J. Hunn, and J. Miller, J. Nucl. Mater. **372**, 400 (2008).
[12] M. Mendelev, H. Zhang, and D. Srolovitz, J. Mater. Res. **20**, 1146 (2005).
[13] C. Minkwitz, C. Herzig, E. Rabkin, and W. Gust, Acta. Mater. **47**, 1231 (1999).
[14] G. Meric de Bellefon and B. D. Wirth, J. Nucl. Mater. **413**, 122 (2011).
[15] S. J. Plimpton, J. Comp. Phys. **117**, 1 (1995).
[16] J. Tersoff, Phys. Rev. B. **39**, 5566 (1989).
[17] C. Kohler, Phys. Stat. Sol. B **234**, 522 (2002).
[18] M. Wojdyr, S. Khalil, Y. Liu, and I. Szlufarska, Model. Simul. Mater. Sc. **18**, 075009 (2010).
[19] I. Szlufarska, A. Nakano, and P. Vashishta, Science **309**, 911 (2005).

[20] K. Tanaka and M. Kohyama, J. Electron Microscopy **51**, 265 (2002).
[21] K. Tanaka and M. Kohyama, Phil. Mag. A **82**, 215 (2002).
[22] M. Kohyama and R. Yamamoto, Mater. Res. Soc. Symp. P. **339**, 9 (1994).
[23] P. Pirouz and J. Yang, Mater. Res. Soc. Symp. P. **183**, 173 (1990).
[24] K. Tanaka, M. Kohyama, and M. Iwasa, Mater. Sci. Forum. **294**, 187 (1999).
[25] G. Kresse and J. Hafner, Phys. Rev. B. **48**, 13115 (1993).
[26] G. Kresse and J. Hafner, J. Phys-Condens. Mat. **6**, 8245 (1994).
[27] G. Kresse and J. Furthmüller, Phys. Rev. B. **54**, 11169 (1996).
[28] G. Kresse and J. Furthmüller, Comput. Mater. Sci **6**, 15 (1996).
[29] P. E. Blöchl, Phys. Rev. B. **50**, 17953 (1994).
[30] G. Kresse and D. Joubert, Phys. Rev. B. **59**, 1758 (1999).
[31] H. J. Monkhorst and J. D. Pack, Phys. Rev. B. **13**, 5188 (1976).
[32] J. P. Perdew, K. Burke, and M. Ernzerhof, Phys. Rev. Lett. **77**, 3865 (1996).
[33] R. Borg and G. Dienes, *An introduction to solid state diffusion*, 1st ed. (Academic Press London, London, 1988).
[34] C. Van de Walle and J. Neugebauer, J. Appl. Phys. **95**, 3851 (2004).
[35] I. Kaur, Y. Mishin, and W. Gust, *Fundamentals of grain and interphase boundary diffusion* (John Wiley and Sons, Ltd., 1995).
[36] H. Nabielek, P. Brown, and P. Offermann, Nucl. Technol.;(United States) **35**, 483 (1977).
[37] W. Amian and D. Stover, Nucl. Technol **61**, 475 (1983).
[38] N. Peterson, J. Vac. Sci. Technol. A. **4**, 3066 (1986).
[39] B. Cordero, V. Gomez, A. E. Platero-Prats, M. Reves, J. Echeverria, E. Cremades, F. Barragan, and S. Alvarez, Dalton Trans. **21**, 2832 (2008).
[40] T. Kwok, P. S. Ho, and S. Yip, Phys. Rev. B. **29**, 5363 (1984).
[41] H. Mehrer, *Diffusion in solids: Fundamentals, methods, materials, diffusion-controlled processes* (Springer, 2007).
[42] H. Nabielek (33rd ICACCS discussion group of symposium 10 on silicon carbide, Daytna Beach, FL, 2009).
[43] K. Verfondern, R. Moormann, and R. Martin, Forschungszentrum Juelich GmbH (1993).
[44] A. H. Booth, *A method of calculating fission gas diffusion from UO_2 fuel and its application to the X-2-f loop test*, Tech. Rep. (Atomic energy of Canada Ltd. Chalk River Project, Chalk River, ONT, 1957).
[45] G. L. Harris, *Properties of Silicon Carbide* (Institution of Engineering and Technology, 1995).
[46] D. A. Petti, S. B. Grover, and J. T. Maki (ASME, 2008).
[47] H. J. MacLean, *Silver transport in CVD Silicon Carbide*, Ph.D. thesis, Massachusetts Institute of Technology (2004).
[48] R. Gontard and H. Nabielek, *Performance evaluation of modern HTR TRISO fuels*, Tech. Rep. (Forschungszentrum Julich GmbH, Julich, Germany, 1990).
[49] R. Lauf, T. Lindemer, and R. Pearson, J. Nucl. Mater. **120**, 6 (1984).
[50] E. S. McGarrity, P. M. Duxbury, and E. A. Holm, Phys. Rev. E. **71**, 026102 (2005).
[51] D. Stauffer and A. Aharony, *Introduction to percolation theory* (Taylor and Francis, London, 1994).